CFD Letters

Computational Fluid Dynamic (CFD) Analysis of Parachute Canopies Design for Aludra SR-10 UAV as a Parachute Recovery Systems (PRS)

Open Access

Raudhah Saim[1*], Sofian Mohd[1], Syariful Syafiq Shamsudin[1], Mohd Fadhli Zulkafli[2], Siti Nur Mariani Mohd Yunos[2], Muhammad Riza Abd Rahman[3]

1   Aircraft System and Design Research Group (ASDR), Universiti Tun Hussein Onn Malaysia, Malaysia
2   Aerodynamics and Propulsion Research (APR), Universiti Tun Hussein Onn Malaysia, Malaysia
3   Unmanned Systems Technology Sdn. Bhd., DRB-HICOM Defence Technologies (HQ), Shah Alam, Selangor, Malaysia

ARTICLE INFO	ABSTRACT
	Unmanned Systems Technology (UST) Aludra SR-10 Unmanned Aerial Vehicle (UAV) was purposely designed for survey and mapping mission. In the early design stage of Aludra SR-10 UAV, skid and belly landing method was used as a recovery method. This type of landing method may encounter a harsh landing on hard soil and gravel, producing high impact momentum on the aircraft body and may cause structural or system damage. To increase the safety of Aludra SR-10 UAV operation, Parachute Recovery System (PRS) are purposely design to replace the belly landing technique for landing method. This study was performed by simulation approach (using Computational Fluid Dynamic, CFD) to analyse an aerodynamic performance for selecting the best canopy design that can produce higher drag during recovery process. This computational study focuses on an aerodynamic flow simulation over three-dimensional surface on two different canopy designs (i.e. annular canopy and cruciform canopy), and also focuses on drag coefficient in a steady and turbulent condition. Two-equation k-ε turbulence flow was modelled by adopting Navier-Stokes numerical equations to simulate aerodynamic characteristics and drag. The computational results with an efficient grid study shows an annular parachute canopy produced highest drag coefficient (1.03) than cruciform parachute canopy (0.91). The findings also highlighted the significance of separation and recirculating flows behind studied geometries, which in turn was responsible in producing the drag. This computational simulation analysis successfully provided a baseline annular parachute design was about 2.41 meter of the nominal diameter was selected as the main parachute which can be applied for this research.

1. Introduction

Recovery are often described as the most difficult and critical phases in UAV operations. The primary function of the recovery system is to land the UAV on a runway, smooth field road, or carrier

---

* *Corresponding author.*
E-mail address: iedaraudhah@gmail.com (Raudhah Saim)

deck safely. Proper and suitable design of the recovery system for UAVs is highly desirable factor to prevent improper landing that may lead to accidents. There are various types of recovery system that available for the small-to-medium AVs such as skid or belly recovery, wheeled landing, parachute recovery and vertical-net recovery. However, different technologies for recovering present together with positive and negative attributes [1–4].

Nowadays, Parachute Recovery System (PRS) are recently used for landing method purposely to replace the belly landing technique. The PRS mechanism are currently applied in numerous tasks in aviation industry and very suitable to be applied as recovery system in small and medium sized unmanned aircraft such as Aludra SR-10 UAV. Prior to the study, several important parameters were considered which included parachute shape, canopy sizing and descent rate.

There are four shapes of parachute design that have been commonly used as recovery system for UAVs i.e. cruciform, hemisphere, annular and parafoil shape. Different configuration of parachute possesses different flow field characteristics. These various shapes of parachutes create different drag forces and behavior during descending. The parachute create higher drag force, thus provide a better performance better than the one with less drag force [5,6]. Due to the shape design and steerable characteristics of the parafoil canopy, this type of parachute was unnecessarily to be investigated in this current work. Since the annular canopy parachute (equipped with vent hole at the apex of parachute that allowed air flow through it in order to avoid large force) can descend faster and produce more drag than the solid hemisphere canopy parachute, therefore only annular and cruciform parachute were emphasized in developing an optimized model.

The parachute sizing is the most important factor for determination of the baseline size of parachute based on aircraft weight to ensure stable and uniform descent behaviour. If the parachute is too small, the aircraft will descend in a higher rate which may damage upon landing. On the contrary, larger parachute with greater surface area will descend slowly leads to a delayed descent time as well longer landing distance due to dragging by the wind. Additionally, the larger parachute (based on the aircraft's weight) will cause the parachute lose the dome shape or crumpling and consequently the effective area is reduced.

Investigating the parachute recovery has continued to the finding of an important contribution of the descent rate to the system. Randall [7] identified and classified two types of parachute's descent rate, slow and fast descent rate. The parachute called as parachute's fast descent rate when the descent rate at 4.5 m/s, while it called as a low descent when the rate of descent is 3.5 m/s. Each descent rate related to the drag coefficient C_D, between 0.75 and 1.5.

Modelling of baseline parachute size of Aludra SR-10 UAV is very important in this research work using simulation and aerodynamic analysis. For the purpose of this problem, a Computational Fluid Dynamic (CFD) software called ANSYS – FLUENT software were used in order to compare the performance of different parachute design. An aerodynamic and flow field over the parachute canopy were study for better analysis and understanding of inflated characteristics of the parachute. Based on the evaluation of the parachute design selection that have been made previously, the aerodynamic performance of two types of parachute design called as annular and cruciform parachute were evaluated using this software. The parachute which provide the higher drag force will be chosen as the parachute for the PRS of Aludra SR-10 UAV.

2. Methodology

In this computational simulation study, the aerodynamic analysis carried out in this present work involves two different geometry analysis that is analysis on

   i.   The parachute configuration alone

   ii. The combined parachute – aircraft configuration.

The first condition dealt with an analysis of the aerodynamic characteristics and performance over three-dimensional surface on two different canopy designs (i.e. annular canopy and cruciform canopy). On the other hand, two different recovery designs where the annular and cruciform parachute were connected to the aircraft was defined as recovery phase which was used for the second simulation condition.

2.1 Parachute Models

An earliest reference, as well as a principle resource for these system was written by Knacke [8] in "The Parachute Recovery Systems Design Manual". The parachute design manual provide a guideline to evaluate, select, design, manufacture, test and operate the recovery parachute. The 3D inflated geometry model was designed based on the physical parameters that were calculated according to Knacke's guideline. Solidwork software was adopted to construct an approximate shape of a fully inflated annular and cruciform parachute based on the canopy sizing theory. Parameters were standardized for both canopy designs to have a feature on the same scale of the analysis study (Table 1). The inflated shape of canopy has relationship between the nominal diameter (D_o) and the inflated shape projected diameter (D_p). Constructed shape defines constructed diameter (D_c) and cross section (nominal diameter) of the parachute canopy.

This study was extended with 25% of parachute changes either smaller or larger than baseline diameter size for better understanding of the parachute aerodynamic performance as a function of diameter change. Three geometry models were used in CFD analysis for each parachute types to recovery of 5kg UAV. All calculated data were tabulated in Table 2 and the conceptual geometry for both inflated parachute canopies is shown in Figure 1.
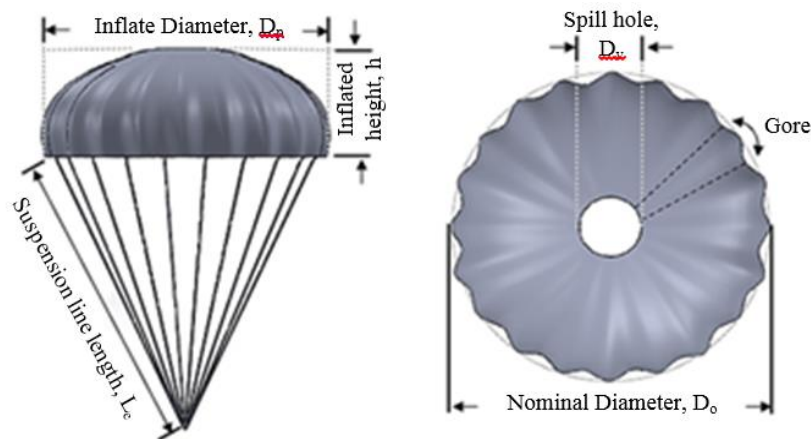
Table 1
Design parameter guideline

Parachute design	Inflated shape, D_p/D_o	Drag coefficient , C_d
Annular	0.66	0.87
Cruciform		0.85

Table 2
Parachute dimension data

Dimension	Annular Parachute			Cruciform Parachute		
	Design A_1	Design B_1	Design C_1	Design A_2	Design B_2	Design C_2
Nominal diameter, Do (m)	1.80	2.41	3.01	2.17	2.89	3.62
Inflated shape diameter, D_P (m) = 0.66 Do	1.19	1.59	1.98	1.43	1.91	2.39
Inflated height, h (m) = 0.3 D_O	0.54	0.72	0.90	0.65	0.87	1.08
Spill hole diameter, D_V (m) = 0.1 D_O	0.18	0.24	0.30			
Suspension lines length, Le (m) = 1.0 D_O	1.80	2.41	3.01	2.17	2.89	3.62
Arm width, W (m) = 1/3 D_O				0.72	0.96	1.21

Note: * Design A: 25% less than baseline diameter
                  * Design B: Baseline diameter
                  * Design C: 25% larger than baseline diameter

(a) Annular parachute

(b) Cruciform parachute
Fig. 1. Conceptual design of inflated parachute

3. Numerical Setup

The setup used in the numerical analysis is further explained in this section.

3.1 Flow Domain

In a CFD external flow analysis, the flow domain was subdivided into inlet, outlet and far-field boundary. The proper sizing of atmospheric wind domain where simulated wind flowed was considerably important because it affected the pressure distribution around the structure or obstacle model. The stationary region of the inlet, outlet and far-filed boundary were located far enough from the geometrical model to prevent recirculation and spoil smooth flow that might induce convergence problems. The size of the computational domain must was typically at least larger than the actual scales of geometry model [9].

The cylindrical shape domain was used to obtain uniform flow simulation. In the first condition study, the simulation on parachute canopies were conducted to validate the geometry design. The inlet and outlet boundaries were located $2D_o$ from upstream and $7D_o$ from downstream of the origin of the parachute position. For the external flow domain, the enclosure radius was set as $5D_o$ where D_o was referred to the nominal diameter of parachute (D_o). The stationary domain for both cases was presented in Figure 2.

In the second case, the stationary domain was setup vertically to represent the descent phase of recovery system. Here, a fully inflated recovery parachute was implemented to the aircraft without suspension lines to reduce complexity of the simulation. The length between aircraft and parachute was the length of suspension line (L_e). Note that, the drag coefficient for the computed flow of the static parachute canopy will be greater with accounting the suspension lines drag contribution [10] The size of domain depended on the length between aircraft and parachute, indicated as C. Figure 3 show the parachute stationary domain.
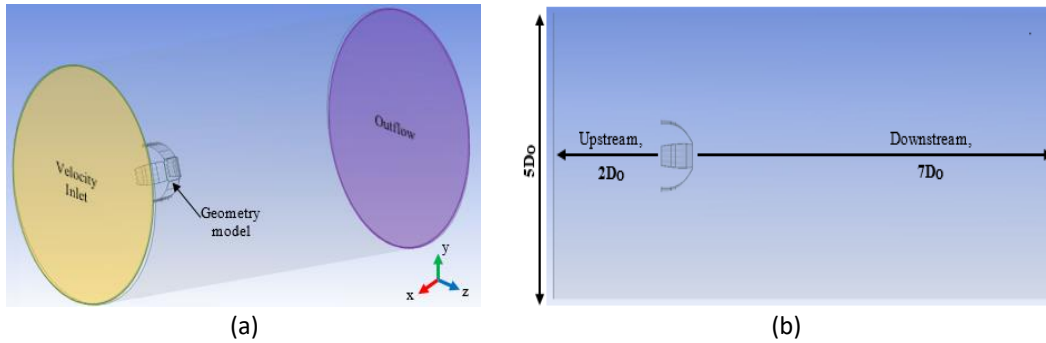

(a)   (b)

Fig. 2. Flow domain and boundary condition for the first case study of (a) stationary domain and boundary condition include an inlet, outlet, geometry model and stationary domain; (b) parachute domain
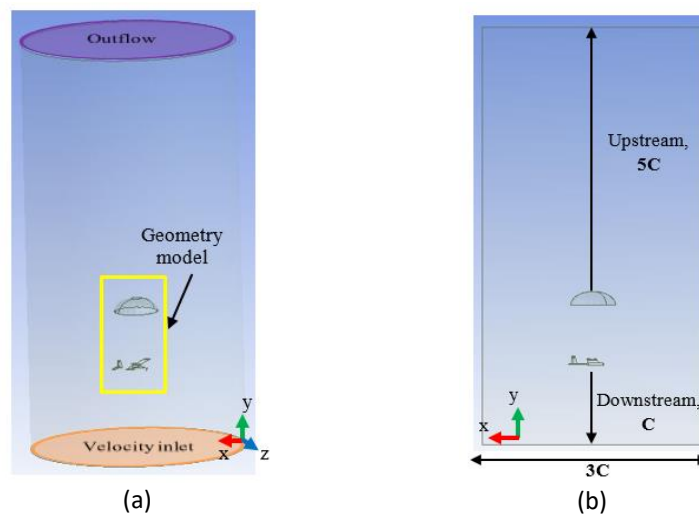

(a)   (b)

Fig. 3. Flow domain and boundary condition for the second case study of (a) stationary domain and boundary condition include an inlet, outlet, geometry model and stationary domain and; (b) recovery domain

3.2 Mesh Generation

The quality of meshing plays an important role in sustaining stability and accuracy of the CFD simulation. In this study, three unstructured meshes with different grid resolution types were generated and compared among various grids included: coarse, medium and fine grids. The grid meshing was generated without any adjustment. Fully unstructured tetrahedral elements grip of the mesh were generated for all geometry model. These complex geometries were discretize using proximity and curvature size element with high capabilities to mesh on the complex surface geometries. Figure 4 and Figure 5 present the surface mesh of aircraft geometry, parachute

geometries and parachute recovery geometries for both cases. The cell size near the geometries model was smaller and gradually increased toward the stationary domain region. The selection of suitable meshing type for these analyses was evaluated based on the skewness value. Indeed, the meshing and smoothing geometry surface values mainly influenced the model simulation that reached stationary solutions and reduced computational efforts.
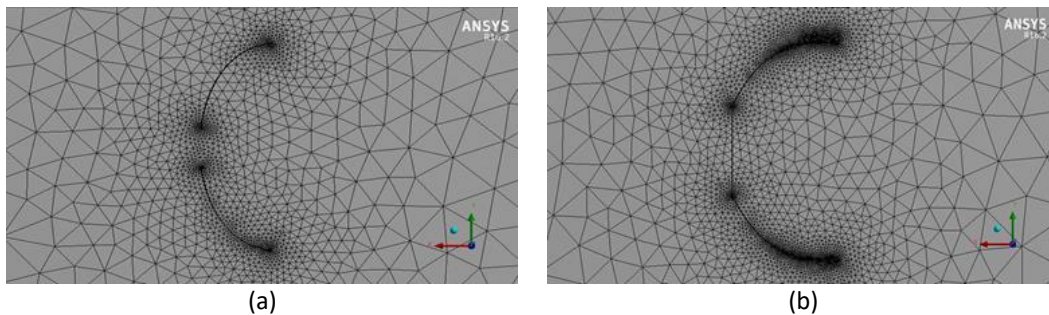

| (a) | (b) |

Fig. 4. Surface mesh on geometries model in the first case study (a) mesh on the annular canopy and; (b) mesh on the cruciform canopy
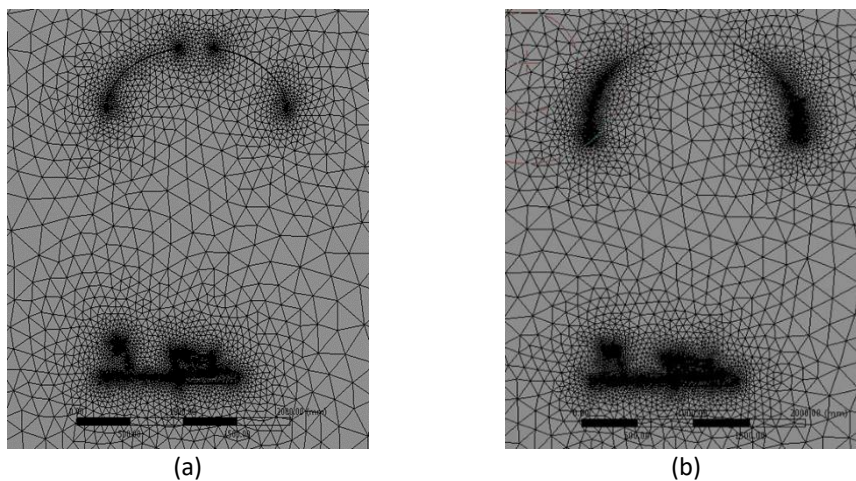

| (a) | (b) |

Fig. 5. Surface mesh on geometries model in the second case study. The cell sizes near the geometry model are smaller and increase toward the outer boundary. (a) mesh on an annular parachute recovery and (b) mesh on the cruciform parachute canopy

3.3 Boundary Condition

There is no benchmark of experimental data to verify the fidelity either computational structural or fluid dynamic solution for the parachute studies. However, several researchers have compared the simulation and experimental study on parachute design. Based on the previous study, RNG k-ε turbulence model simulation showed the closest result with the experimental data. The k-ε RNG model was also known as it produced less viscous flow that led to create more realistic flow and higher accuracy in the simulation of complex geometry and swirling flow [11–13]. Therefore, k-ε RNG model was used in this simulation.

Both simulations were developed to represent the flow inside the wind tunnel with constant wind speed around the solid aircraft and inflated dome-shaped canopies. This simulation was assumed at 100 meter AGL. Since the study was conducted under turbulent free-flow conditions, density of air was assumed constant as the air temperature did not significantly affect the parachute in this flow

condition. As the air density was constant, the flow was considered as incompressible and simulated using pressure-based solver.

The no-slip boundary condition was applied on the geometry model, so that, the fluid velocity at fluid-solid surface boundaries was equal to the solid boundary. Iteration was stop when solution was remained constant or the solution was converged. Besides that, assumptions of the descent rate of parachute were made. Faster descent rate provided a useful short time to reach the ground and avoid the aircraft to land farther than the predicted landing point. Therefore, high speed descent rate of 4.5 m/s provided by Randall [7] study was selected in this study.

4. Numerical Method Verification and Validation

Validation is a process of evaluating the accuracy and reliability of geometry model in computational simulations. Model accuracy was accessed using a grid refinement analysis called as Grid Convergence Index (GCI). The necessity of a grid refinement not only has significance on the solution accuracy, but it also offers an effect on a convergence speed. The details of grid generated for each domain were discussed in separate section.

4.1 Parachute Geometry

Three unstructured meshes around two baseline parachute canopies using five prism layers were generated for the grid convergence study included coarse, medium and fine grids. The mesh details and grid resolutions for baseline parachute were detailed in Table 3 and presented in Figure 6 and Figure 7, including prism layer thickness (Δs) that was selected in a region near parachute surface to resolve boundary layer features.

From this current finding, the foregoing grid convergence study using a fine grid resolution was found to be sufficient to resolve this simulation. The details of meshing resolution for all parachute design were presented in Table 4. The three-dimensional Navier-Stokes equation of incompressible flow was solved numerically using the standard k-ε turbulent model as a transport equation to represent the turbulent properties of the fluid flow around the parachute.

Table 3
Details of the unstructured grids around baseline parachute canopy

Canopy design	Δs (mm)	Mesh	Nodes	Elements	Skewness
Annular, A_1		Coarse	62 662	348 573	0.8425
	9.0402×10^{-5}	Medium	71 634	401 041	0.8329
		Fine	95 231	413 376	0.8457
Cruciform, A_2	8.9320×10^{-5}	Coarse	182 115	995 880	0.8406
		Medium	317 162	1 264 862	0.8426
		Fine	347 393	1 912 503	0.8439

Table 4
Details of the unstructured grids around canopy design

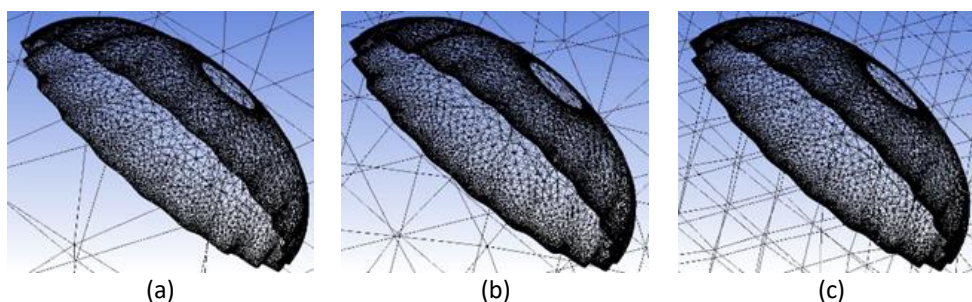| Design	Annular canopy			Cruciform canopy		
	A_1	B_1	C_1	A_2	B_2	C_2
Nodes	63 559	95 231	131 451	145 042	347 393	360 796
Elements	348 105	413 376	734 736	790 419	1 912 503	1 999 767
Skewness	0.8138	0.8457	0.8470	0.8328	0.8439	0.8471

Fig. 6. Unstructured viscous grids around the annular canopy of (a) coarse meshing; (b) medium meshing and; (c) fine meshing
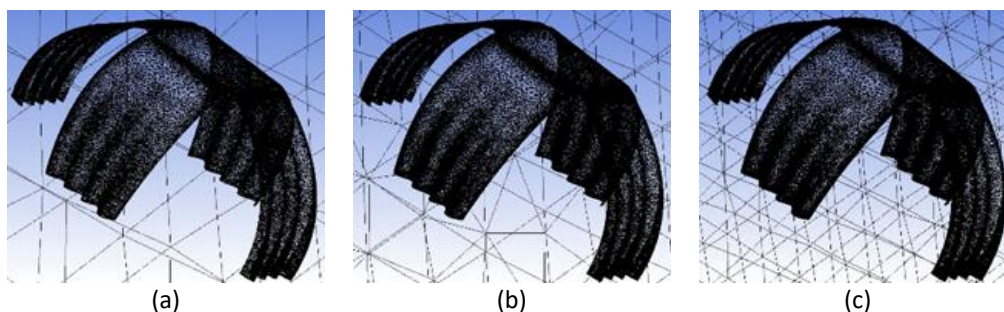

Fig.7. Unstructured viscous grids around the cruciform canopy of (a) coarse meshing; (b) medium meshing and; (c) fine meshing

4.2 Recovery System Geometry

Three unstructured meshes around two baseline parachute canopies` were generated for the Grid Convergence Index (GCI) test: coarse, medium and fine grids. The details of mesh resolution were given in Table 5. Based on this grid independence test, fine and medium grid resolution was selected for annular and cruciform canopy simulation, respectively (present in Figure 8). Optimum and fine grid resolution was needed to lower the grid resolution and reduce computational running time. Additionally, the details of meshing resolution for all recovery parachute design were presented in Table 6.

Table 5
Details of the unstructured grids around baseline recovery parachute

Canopy design	Mesh	Nodes	Elements	Skewness
Annular, A_1	Coarse	97 518	540 815	0.8492
	Medium	196 748	1 093 336	0.8486
	Fine	348 827	1 572 601	0.8691
Cruciform, A_2	Coarse	190 890	1 048 989	0.8290
	Medium	381 773	2 107 162	0.8786
	Fine	613 462	3 401 169	0.9105

Table 6
Details of the unstructured grids around recovery parachute

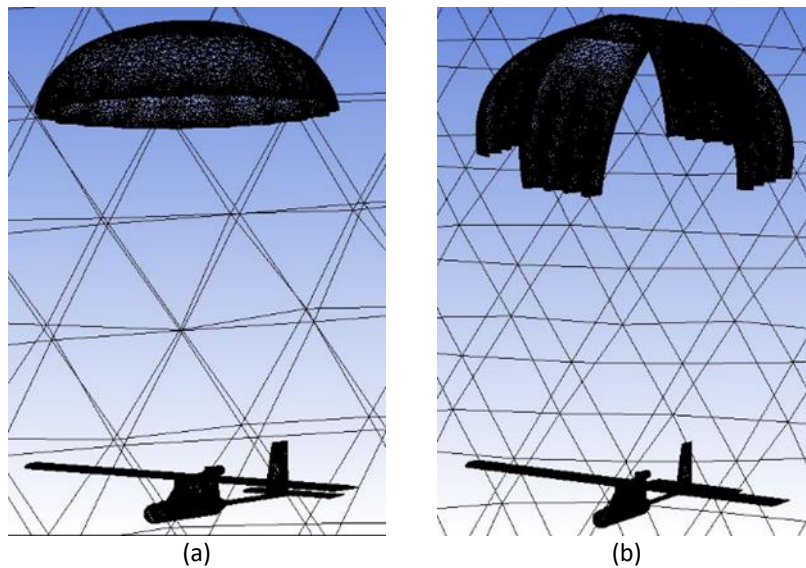| Design	Annular canopy			Cruciform canopy		
	A_1	B_1	C_1	A_2	B_2	C_2
Nodes	146 265	348 827	354 132	267 050	381 773	588 558
Elements	636 535	1 572 601	1 941 187	1 200 119	2 107 162	2 902 623
Skewness	0.8377	0.8691	0.9002	0.8539	0.8786	0.9370

(a)   (b)

Fig. 8. Unstructured viscous grids around the recovery system of (a) fine meshing for baseline annular recovery system and (b) medium meshing for baseline cruciform recovery system

5. Results and Discussions

Details of the results included a flow field and performance were discussed in separate section.

5.1 Parachute Geometry

The physical view of the flow-field around both parachute canopies showed an aerodynamic of parachute was considerably unsteady flow behind the parachute. The unsteady flow was caused by the complex interaction between canopy design and air flow which resulted in a separated flows and vortex shedding. Figure 9(a) shows the main topological flow structure of the annular parachute was described by the flow pattern around parachute canopy. The high speed of air release from inlet was directly flow toward the inflated parachute. As the air approaching the parachute's stagnation point, the velocity of air was gradually decreased. When the air entered the parachute domain, most of the airflow could not escape or get through the canopy due to solid and non-porous type of parachute. There are also air was directly passing through the vent hole at the apex while some went along the canopy's surface before separating and leaving at the skirt edge. This phenomenon resulted in a turbulence separation flow. On the other hand, the topological flow structure of cruciform parachute displayed the air flow was jetted not only through the edge skirt but also through the slots between parachute arms just after the air reach the apex (Figure 9(b)). Once the air began to separate, a wake flows separation was directly created and reattached behind the canopy with the net that led to a formation of vortex shedding. The formation of vortexes called uniform wake flow was responsible for increasing the drag force [8,14,15].

Apparently, the differential of pressure formation between the parachute's internal domain and outer surface was the most significant finding. The positive and negative pressure formed a strong outwardly pressure gradient that sustained the canopy to be inflated and stable during the descent, so-called as pressure drag. A comparison data of pressure distribution for both parachute shapes were details in Figure 10. As the fluid moved from high to low pressure, the fluid moved from higher pressure that was forced toward the lower pressure region by Bernoulli principle. The pressure difference existed due to the surface area changes between spill hole, skirt edge and arm's slot with

the surrounding. In short, the pressure increased as the fluid decelerated when approaching parachute domain and started to accelerated at the edge of parachute with decreasing pressure.

The details of the drag coefficient, C_d result for all parachute design were presented in Table 7. According to the simulation, the annular parachute produced higher drag coefficient (C_d) than the cruciform parachute. Furthermore, the present finding showed the drag coefficient generated was increased as a function of parachute size. By increasing the nominal diameter of parachute, high pressure distribution was generated at the wake region.

Table 7
Simulation result of canopy design

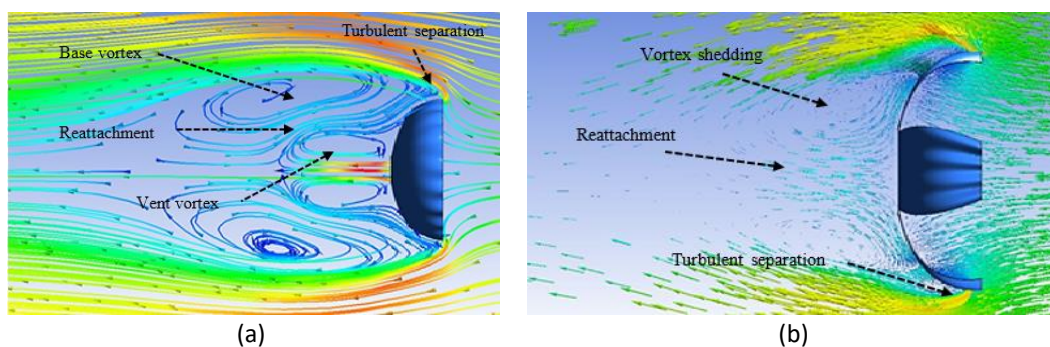| Parachute design	Annular canopy			Cruciform canopy		
	A_1	B_1	C_1	A_2	B_2	C_2
C_d	0.7875	0.7915	0.8039	0.7836	0.7855	0.7970

Fig. 9. Velocity gradient around parachute (a) annular parachute; (b) cruciform parachute
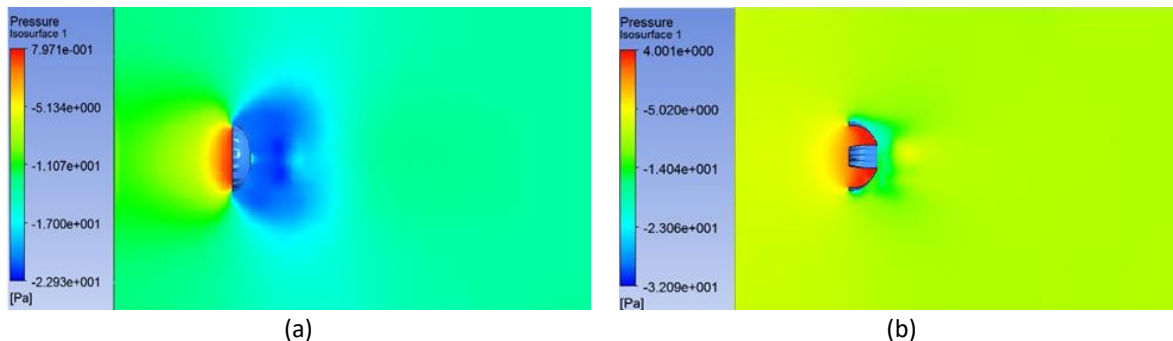

Fig. 10. Pressure distribution around parachute (a) annular parachute; (b) cruciform parachute

5.2 Parachute Recovery Geometry

Figure 11 illustrated visualizations of velocity flow structure around the aircraft and parachute model at a steady state descent. The high speed of air releases from the inlet was directly flowed toward aircraft before entering into the inflated parachute. This condition affecting the flow structure and aerodynamic properties above the aircraft's wing [16]. As the air flowed over the aircraft's wing, the velocity of air was decelerated until zero as it approached the stagnation point which clearly lower than free stream velocity. In the meantime, air began to swirl and form a wake region as it approached the parachute domain. As discussed previously, the airflow moved around the internal part of the parachute domain, then, separated and left either at skirt edge, vent hole or slots between arms of the parachute. Unsteady flow field was directly created behind the canopy with the net, consequently created the vortex shedding.

Further research was performed to examine thoroughly the links between formations of pressure and drag on the recovery system. The details of the drag coefficient (C_d) for all recovery parachute design were presented in Table 8. The pressure difference between the internal and external surfaces of parachute was responsible for increasing the drag force that allowed the parachute to stay aloft. This relationship was called as pressure drag. As compared to the cruciform canopy, the annular canopy produced higher pressure difference over recovery system which indicated that a larger pressure drag was generated. In this simulation, annular canopy produces higher drag coefficient compared to cruciform canopy during descent phase. Moreover, the result attained showed a significant increase in pressure distribution as well as the drag coefficient when parachute diameter were increased.

Table 8
Simulation result of parachute recovery

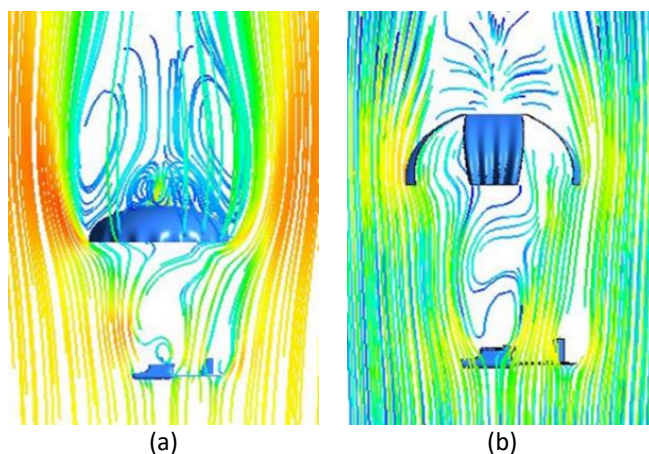| Parachute Design	Annular canopy			Cruciform canopy		
	A_1	B_1	C_1	A_2	B_2	C_2
C_d	1.00	1.03	1.11	0.86	0.91	1.02

(a)   (b)

Fig. 11. Velocity profile around parachute recovery (a) annular parachute; (b) cruciform parachute

6. Conclusion

The computational simulation analysis successfully provided the best canopy design which can be applied for this research. A baseline annular parachute canopy was about 2.41 meter of the nominal diameter was selected as the main parachute, which produced highest drag coefficient (1.03). The findings also highlighted the significance of separation and recirculating flows behind studied geometries, which in turn was responsible in producing the drag. The selected parachute was undergone a drop test before undertaking into a flight test to determine a feasibility and ability of the parachute to support Aludra SR-UAV and bring to safe landing.

Acknowledgement

References

[1] R. Abinaya and R. Aravind. "Selection of low-cost recovery system for Unmanned Aerial Vehicle." *International Research Journal of Engineering and Technology* 4, no. 5 (2017): 1074–1078.

[2] Gundlach, Jay. *Designing unmanned aircraft systems: a comprehensive approach*. American Institute of Aeronautics and Astronautics, 2012.

[3] Fahlstrom, Paul, and Thomas Gleason. *Introduction to UAV systems*. John Wiley & Sons, 2012.

[4] Beard, Randal W., and Timothy W. McLain. *Small unmanned aircraft: Theory and practice*. Princeton university press, 2012.

[5] Cockrell, David J., and A. D. Young. "The aerodynamics of parachutes." (1987).

[6] Stein, Keith, Tayfun Tezduyar, Vinod Kumar, Sunil Sathe, Richard Benney, Eric Thornburg, Clifton Kyle, and Tomoyasu Nonoshita. "Aerodynamic interactions between parachute canopies." *J. Appl. Mech.* 70, no. 1 (2003): 50-57.

[7] S. Randall. "Parachute Sizing Chart." *UKHAS wiki*. UK High Altitude Society, 2001.

[8] Knacke, Theo W. *Parachute recovery systems design manual*. No. NWC-TP-6575. NAVAL WEAPONS CENTER CHINA LAKE CA, 1991.

[9] D. Feszty and T. Jakubík. "NGM_JF006_1: Computational Fluid Dynamics." 2017.

[10] Stein, Keith R., Richard J. Benney, Tayfun E. Tezduyar, John W. Leonard, and Michael L. Accorsi. "Fluid-structure interactions of a round parachute: Modeling and simulation techniques." *Journal of Aircraft* 38, no. 5 (2001): 800-808.

[11] A. Bakker. *Applied Computational Fluid Dynamics*. 2001.

[12] Hou, Qinfu, and Zongshu Zou. "Comparison between standard and renormalization group k-ε models in numerical simulation of swirling flow tundish." *ISIJ international* 45, no. 3 (2005): 325-330.

[13] Bulat, Mikhail Pavlovich, and Pavel Victorovich Bulat. "Comparison of turbulence models in the calculation of supersonic separated flows." *World Applied Sciences Journal* 27, no. 10 (2013): 1263-1266.

[14] Xing-long, Gao, Zhang Qing-bin, Tang Qian-gang, and Yang Tao. "Fluid-structure interaction simulation of parachute in low speed airdrop." In *Proceedings of the World Congress on Engineering*, vol. 3, pp. 3-5. 2013.

[15] Cao, YiHua, Kan Wan, QianFu Song, and John Sheridan. "Numerical simulation of parachute Fluid-Structure Interaction in terminal descent." *Science China Technological Sciences* 55, no. 11 (2012): 3131-3141.

[16] Zain, Nadhirah Mohd, Shabudin Mat, Khushairi Amri Kasim, Shuhaimi Mansor, Md Nizam, and Norazila Othman Dahalan. "Wind tunnel experiments on a generic sharp-edge delta wing UAV Model." *Journal of Advanced Research in Fluid Mechanics and Thermal Science* 40, no. 1 (2017): 18-26.